BBA - Molecular Basis of Disease 1865 (2019) 1579–1591

Contents lists available at ScienceDirect

BBA - Molecular Basis of Disease

journal homepage: www.elsevier.com/locate/bbadis

Dystrobrevin is required postsynaptically for homeostatic potentiation at the *Drosophila* NMJ

Salinee Jantrapirom[a,f], Wutigri Nimlamool[a,b], Piya Temviriyanukul[c], Somaieh Ahmadian[d], Cody J. Locke[e], Graeme W. Davis[e], Masamitsu Yamaguchi[f], Jasprina N. Noordermeer[d], Lee G. Fradkin[d,g,1], Saranyapin Potikanond[a,b,d,*,1]

[a] Department of Pharmacology, Faculty of Medicine, Chiang Mai University, Thailand
[b] Research Center of Pharmaceutical Nanotechnology, Chiang Mai University, Thailand
[c] Institute of Nutrition, Mahidol University, Thailand
[d] Laboratory of Developmental Neurobiology, Department of Molecular Cell Biology, Leiden University Medical Center, the Netherlands
[e] Department of Biochemistry and Biophysics, University of California, San Francisco, CA, USA
[f] Department of Applied Biology, Kyoto Institute of Technology, Matsugasaki, Sakyo, Kyoto, Japan
[g] University of Massachusetts Medical School, MA, USA

ARTICLE INFO

Keywords:
Dystrobrevin
Dystrophin
cdc42
Neuromuscular junction
Synaptic homeostasis
Drosophila

ABSTRACT

Evolutionarily conserved homeostatic systems have been shown to modulate synaptic efficiency at the neuromuscular junctions of organisms. While advances have been made in identifying molecules that function presynaptically during homeostasis, limited information is currently available on how postsynaptic alterations affect presynaptic function. We previously identified a role for postsynaptic Dystrophin in the maintenance of evoked neurotransmitter release. We herein demonstrated that Dystrobrevin, a member of the Dystrophin Glycoprotein Complex, was delocalized from the postsynaptic region in the absence of Dystrophin. A newly-generated *Dystrobrevin* mutant showed elevated evoked neurotransmitter release, increased bouton numbers, and a readily releasable pool of synaptic vesicles without changes in the function or numbers of postsynaptic glutamate receptors. In addition, we provide evidence to show that the highly conserved Cdc42 Rho GTPase plays a key role in the postsynaptic Dystrophin/Dystrobrevin pathway for synaptic homeostasis. The present results give novel insights into the synaptic deficits underlying Duchenne Muscular Dystrophy affected by a dysfunctional Dystrophin Glycoprotein complex.

1. Introduction

Homeostatic signaling systems are conserved from insects to humans and are considered to interface with the mechanisms of neural plasticity in order to stabilize neural function [1–3]. These systems have been shown to control diverse cellular processes, including membrane excitability [2,4], postsynaptic neurotransmitter receptor abundance [5,6], and presynaptic neurotransmitter release [1].

At the *Drosophila* neuromuscular junction (NMJ), the loss or pharmacological inhibition of postsynaptic glutamate receptors induces a compensatory increase in presynaptic release that precisely offsets changes in postsynaptic receptor function and maintains normal synaptic excitation in muscle [7,8]. The homeostatic modulation of neurotransmitter release is achieved by parallel increases in presynaptic calcium influx through the CaV2.1 calcium channel [9] and a readily releasable pool (RRP) of synaptic vesicles [10].

Large-scale forward genetic screening has identified several genes encoding presynaptic proteins that, when mutated, block presynaptic homeostasis without altering baseline anatomical or functional NMJ development [10–13]. In contrast, limited information is currently available on how postsynaptic mechanisms contribute to NMJ synaptic homeostasis, for example, machinery sensing synaptic perturbations and the retrograde signal sent to elicit presynaptic responses.

Dystrobrevin (Dyb), a postsynaptic protein, is a component of the large Dystrophin Glycoprotein Complex (DGC) [14]. It was found to interact with Dystrophin (Dys) at the Torpedo electric organ postsynaptic membrane [15]. We previously reported roles of the postsynaptic localization of DLP2, the large Dys isoform expressed

* Corresponding author at: Department of Pharmacology, Faculty of Medicine, Chiang Mai University, Thailand
E-mail address: saranyapin.p@cmu.ac.th (S. Potikanond).
[1] These authors equally contributed to this work.

https://doi.org/10.1016/j.bbadis.2019.03.008
Received 6 September 2018; Received in revised form 14 March 2019; Accepted 19 March 2019
Available online 21 March 2019
0925-4439/ © 2019 Elsevier B.V. All rights reserved.

throughout muscle fibers, in maintaining normal levels of neurotransmitter release at the *Drosophila* NMJ [16]. The absence of Dys-DLP2 from the subsynaptic reticulum (SSR) results in a high quantal content (QC; the number of transmitter quanta released per nerve impulse), increased numbers of T-bars (presynaptic release sites), and an elevated probability of release [16]. These effects occur in the absence of visible alterations to the localization, density, and function of postsynaptic neurotransmitter receptors. The absence of Dys also results in reduced activity or levels of the Rho-GAP cross-veinless-c (Cv-c) [17], which enhances the conversion of active GTP-bound Rho-GTPases to their inactive GDP-bound forms [18]. The Rho-GTPase, Cdc42, was identified as the substrate of Cv-c at the NMJ and evidence was obtained to show that elevated Cdc42 activity is required for increased QC [17]. However, the potential roles of DGC and the Cdc42 pathway in homeostatic responses remain unclear.

We herein demonstrated that postsynaptic DGC plays an important role in the retrograde suppression of RRP sizes and is required for the expression of presynaptic homeostatic compensation, which occurs upon the acute inhibition of the postsynaptic glutamate receptor field. We extended our previous findings by showing that the loss of Dyb from the SSR results in the abnormal enhancement of presynaptic neurotransmitter release in the *Dystrophin DLP2* mutant (Dys^{Df}). We confirmed that Cdc42 is a primary postsynaptic target of this pathway and demonstrated that the postsynaptic expression of constitutively-active Cdc42 alone is sufficient to increase neurotransmitter release. We further showed that Cdc42 is enriched in the SSR, at which Dyb is also localized. Our results revealed a novel postsynaptic pathway of highly conserved proteins controlling presynaptic neurotransmitter release and homeostasis at synapses. The present result may contribute to identifying the mechanisms responsible for the synaptic impairments exhibited by a significant number of DMD patients.

2. Materials and methods

2.1. Fly stocks

w^{1118}, the genetic background strain of the *Dyb* mutation (Dyb^{11}), was used as the wild-type control genotype for all experiments. The following mutants, drivers, and UAS transgenics were used and are described at Flybase: the *Df(3R)Exel6184* deficiency (Dys^{Df}) that uncovers the entire Dys locus; *Df(2R)Exel6061* and *Df(2R)aichi*^{4}, overlapping deficiencies that uncover the *Dyb* gene; $Cdc42^4$ [19] and $Cv\text{-}c^1$ [17], loss-of-function and hypomorphic alleles, respectively; *24B-GAL4*, *Mhc-GAL4*, *elav-GAL4*, and *OK6-GAL4*, drivers obtained from the Bloomington stock center; *UAS-Cdc42*^{V12} [20] and *UAS-GFP-Cdc42*^{WT} [21]. Heat shock-regulated FLP and FLP/ISce1 lines were used in the generation of the *Dyb* mutant. A transgenic RNAi line targeting *cdc42* mRNA (ID 100794) was obtained from the Vienna *Drosophila* RNAi Center. *UAS-Dyb-PA*-encoding sequences were PCR amplified from wild-type embryonic first-strand cDNA, cloned into the Gateway pENTR vector (Invitrogen), recombined into the pTWM vector (gift from T. Murphey; www.ciwemb.edu/labs/murphy/Gateway%20vectors.html), and introduced into wild-type flies to allow the expression of the MYC-tagged Dyb protein under the control of tissue-specific GAL4 drivers. The 11-amino acid sequence from Shaker that targets heterologous proteins to the SSR [22] was appended to the carboxy-terminus of *UAS-Dyb* A/B by the insertion of an oligonucleotide into the pTWM-*Dyb* A construct described above. All P-element constructs were verified by sequencing. Crosses and the generation of recombinant chromosomes were performed by standard *Drosophila* genetic approaches. We equally selected both male and female to perform all experiments except the electrophysiological recordings that only female was selected.

2.2. Generation of the Dyb mutant by homologous recombination

The *Dyb* gene was targeted by homologous recombination Ends-out targeting [23]. The region encoding the carboxyterminal domain common to all Dyb isoforms was replaced by the *white* gene (Fig. S2B). The targeting construct was generated as follows: *Dyb* homology regions A and C were amplified from wild-type genomic DNA using the primers *Dyb* region A forward, CGTACGCATCATCTGCATTGCTGTCA, *Dyb* region A reverse, GGCGCGCCTAA- GTTCTCAAGACCTAAGT; *Dyb* region C forward, GGTACCGGAGCAGCTCAACAA- GATTA and *Dyb* region C reverse, GCGGCCGCTAGAGCATTTAGAATTTGAT, and TA-cloned into the pGEMT vector (Promega). Homology regions A and C were generated by digests with *Bsi*W1/*Asc*1 and *Acc*651/*Not*1 and ligated into the *Bsi*W1-*Asc*1 and *Acc*651-*Not*1 sites of the pW25 vector (Gong and Golic, 2003), respectively. The construct was transformed into the germ line of w^{1118} flies at BestGene, Inc. Two inserts on the 3rd chromosome were identified and found to be mobilized upon the provision of Flippase. Crosses for targeting were performed at 25 °C. The crossing scheme is shown (Fig. S2A). Genomic DNA from $white^+$ progeny representing potential targeting events was analyzed by PCR using the following primers: F1, TATTGTGCCAGGCATAGGTG: R1, GTGTTT CTCAAGAGC- TGCGC; F2, GCGTAAACC- GCTT GGAGCTTC; R2, CTG GCTCTATGCCGTTACGAT. Other primer sequences are available upon request. Southern blotting was performed to further verify targeting. DNA was prepared from flies homozygous for the putative targeted allele, digested with EcoR1 and Hind3, separated by agarose gel electrophoresis, and then transferred to nylon membranes. The membranes were probed with digoxygenin-labeled homology region A and C DNA fragments and hybridizing fragments were detected using a chemiluminescent assay (Roche).

2.3. Generation of anti-Dys antisera and other immunoreagents

Rabbit antisera were raised against two GST-tagged Dyb antigens: 1) anti-DybCOOH (encoded by base pairs 1842–2408 of the Dyb A transcript, Genbank accession number NM_165904) and 2) anti-DYBmid (encoded by base pairs 1294–1818) at Eurogentec. Other primary antibodies used were anti-actin (MP Biomedicals), anti-horseradish peroxidase (HRP) (Promega), anti-DYSCOOH [16], anti-DLG (DSHB), anti-DGluRIIA (DSHB), anti-DGluRIIB (a gift from A. DiAntonio; [24], anti-Cdc42 (a gift from U. Tepass; [25]) anti-GFP (Molecular Probes, Invitrogen), and anti-Fas2 1D4 [26] and anti-Bruchpilot nc82 (a gift from A. Hofbauer; [27]). Alexa Fluor-conjugated secondary antibodies (Invitrogen) and HRP-conjugated secondary antibodies (Jackson ImmunoResearch Laboratories) were used as described [17]. Standard epifluorescence or confocal microscopy was used to visualize and photograph samples.

2.4. Quantification of bouton numbers

The body walls of third instar larvae were stained with FITC-conjugated anti-HRP (Jackson ImmunoResearch Laboratories). Body wall muscles #6–7 of segments A2-A5 from at least 5–10 larvae (40–80 muscles in total) were used to count the numbers of boutons per synapse.

2.5. Immunohistochemistry

Third instar larvae were dissected in ice-cold PBS, and body walls were fixed in 4% formaldehyde in PBS and then incubated overnight at 4 °C with the anti-Bruchpilot nc82 monoclonal antibody, followed by the application of a goat anti-mouse Alexa Fluor 488 antibody. Body wall synapses were visualized by confocal microscopy (Leica TCS SL, Leica Microsystems), the number of nc82-positive domains at synapses on muscles 6 and 7 in 5 segments (A2–A6) were counted, and the total bouton area was measured and analyzed using Leica Application Suite software.

2.6. Transmission electron microscopy (TEM)

Larval dissection, fixation, embedding, and sectioning were performed as described [16]. Semi-serial sections of body walls from w^{1118} and the Dys^{11} mutant were prepared and electron micrographs were made of Type Ib boutons on muscles 6 and 7 using a transmission electron microscope (Tecnai 12 Biotwin, FEI, Eindhoven, The Netherlands).

2.7. Current-clamp electrophysiology

To minimize possible genetic background effects, we back-crossed each mutant allele or transgenic chromosome against wild-type control flies for at least 5 generations prior to using them in electrophysiological analyses. Electrophysiological recordings were performed as described [17]. Briefly, a microelectrode filled with 3 M KCl was inserted into muscle 6 (segments A3–A4) of dissected third instar female larvae bathed in HL3 containing 0.6 mM Ca^{2+} unless otherwise described. Intracellular measurements were recorded using a Geneclamp 500B amplifier (Axon Instruments, Union City, CA), low-pass filtered at 10 kHz, high-pass filtered at 0.5 Hz, and digitized using Digidata 1322A and pClamp9 software (Axon Instruments). mEJPs were recorded continuously for 1 min. Thirty EJPs were recorded at a 0.3-Hz stimulation after the appropriate axon was stimulated using a pulse generator (Master-8, AMPI, Jerusalem, Israel) via a suction electrode. The electrical input resistance of all muscle fibers recorded was > 4 mΩ. Mean mEJP amplitude and frequency were analyzed using the peak detection feature of Mini-analysis 6.0 (Synaptosoft, Decatur, GA); all events were confirmed by eye. EJP amplitudes were analyzed using Clampfit 9.0 and amplitudes were normalized to a membrane potential of −60 mV. NMJ QC was calculated by dividing the mean EJP amplitude (calculated from 30 events) corrected for non-linear summation (B.A. Stewart, personal communication) by the mean mEJP amplitude (calculated from 100 events). Paired-pulse facilitation (PPF) was assessed at 0.6, 0.4, and 0.2 mM Ca^{2+} using 50-ms interstimulus intervals. All primary electrophysiological data are presented in the Supplemental Tables.

2.8. Philanthotoxin and RRP experiments

Recordings were obtained from muscle 6 in abdominal segment 2 or 3 of wandering third instar larvae with AxoPatch 200B (for current-clamp recordings) or Axoclamp 2B (for two-electrode voltage-clamp recordings), as previously described [10]. Recordings were made in modified HL3 saline at specified calcium concentrations (see figures and text) with the following components (and concentrations): NaCl (70 mM), KCl (5 mM), $MgCl_2$ (10 mM), $NaHCO_3$ (10 mM), sucrose (115 mM), trehalose (5 mM), HEPES pH 7.2 (5 mM), and $CaCl_2$ (0.5 mM for current-clamp recordings and 1.5 mM for two-electrode voltage-clamp recordings). In the acute homeostatic challenge, semi-intact preparations with the central nervous system (CNS), fat, and gut intact were perfused with philanthotoxin-433 (PhTx; Sigma-Aldrich). PhTx was prepared as a stock solution (5 mM in ddH_2O) and diluted in HL3 saline to 15 μM. Following a ten-minute incubation period, dissections were completed and preparations were rinsed and assayed. Muscle input resistance (R_{in}) was monitored at the beginning and end of each recording. Recordings were excluded if R_{in} changed by > 20%. The average single action potential-evoked EJP amplitude (stimulus duration, 3 ms) or EJC amplitude (stimulus duration, 1 ms) for each recording is based on the mean peak EJP amplitudes or EJC amplitudes in response to thirty presynaptic stimuli. QC was estimated for each current-clamp recording by calculating the average EJP/average mEJP, corrected for non-linear summation [28] when noted, and subsequently averaging across all NMJs for a given genotype. To assess the apparent size of the RRP, we applied the method of cumulative EJC amplitudes [10,29,30]. Muscles were clamped to −65 mV, and EJC amplitudes during a stimulus train (60 Hz, thirty stimuli) were calculated as the difference between peak and baseline before the stimulus onset of a given EJC, as previously described [10]. The number of release-ready vesicles was obtained by back-extrapolating a line fit to the linear phase of the cumulative EJC plot (the last 200 ms of a train) to time zero and dividing the cumulative EJC amplitude at time zero by the mean mEJP amplitude recorded in the same cell [10].

2.9. Statistical analyses

The program GraphPad Prism version 5 was used for statistical analyses. A one-way ANOVA was performed with least significant differences (LSD) or Bonferroni for post hoc multiple comparisons. Differences were considered to be significant when $p < 0.05$; *, **, and *** indicate $p < 0.05$, $p < 0.01$, and $p < 0.001$, respectively.

3. Results

3.1. Dyb is delocalized from the NMJ in the absence of Dys

Dyb expression patterns were previously revealed by RNA in situ analyses, indicating that Dyb is expressed in the muscle and nervous system [31]. We generated two different rabbit antisera recognizing epitopes in Dyb common to all isoforms. Specifically, one immunogen, DybCOOH, contained a carboxyterminal region, while the other DybMid, contained sequences encoding the central portion of the protein (see Materials and Methods). The staining of third instar larval body walls with anti-DybCOOH (Fig. 1B) or DybMid (data not shown) revealed that Dyb was present throughout the muscle and was particularly enriched at synaptic boutons (Fig. 1A–C). Dyb was present both pre- and postsynaptically at boutons as evidenced by the high magnification visualization of boutons co-labeled with anti-DybCOOH and the presynaptic marker anti-HRP [32] (Fig. 1A–C).

We then examined whether Dyb is properly localized in the *Dys* mutant background and found that it was no longer localized either pre- or postsynaptically to synaptic boutons in larval NMJ lacking all Dys isoforms (Dys^{Df}) (Fig. 1D–E), indicating that DGC-like complexes, which require Dys, exist at both sides of the synapse. Previously, there were neither study on Dyb roles nor Dyb deficiency affected NMJ. To evaluate the roles of Dyb at the NMJ, we generated a mutant allele of *Dyb*, Dyb^{11}, using “ends-out” homologous recombination [23]. We validated the molecular structure of the knockout by PCR and Southern blotting (Fig. S2C–D). Five out of the seven isoforms' ATG translational initiator codons and the region encoding the domains responsible for Dyb's protein-protein interactions, the EF-hand and ZZ domains [33] (Fig. 1F), were replaced by the mini *white* gene (Fig. S1B) and the Dyb protein was not detectable in Western blot analysis of Dyb^{11} body wall protein extracts (Fig. 1I, upper panel). Thus, Dyb^{11} was almost certainly a null allele of *Dyb*. Homozygous Dyb^{11} was viable and did not display obvious visible phenotypes. Staining of the wild-type third instar larval CNS with anti-Dyb revealed that Dyb was expressed in the neuropile, thoracic neuromeres, and higher order structures in the brain lobes, including the optic system (Fig. 1G). The Dyb^{11} mutant third instar larval CNS did not detectably express Dyb (Fig. 1H). Despite the absence of Dyb from Dys^{Df} larval NMJ, Western blot analyses of Dys^{Df} body wall protein extracts revealed that they still contained normal levels of Dyb (Fig. 1I, middle panel), indicating that the delocalization of Dyb, rather than its degradation, accounts for its absence from the postsynaptic region in Dys^{Df}. We then focused on the postsynaptic functions of Dyb because our previous study on the postsynaptic knockdown of *Dys*, a partner of Dyb, showed excess neurotransmitter release, whereas decreased presynaptic Dys expression had no effect on QC [16].

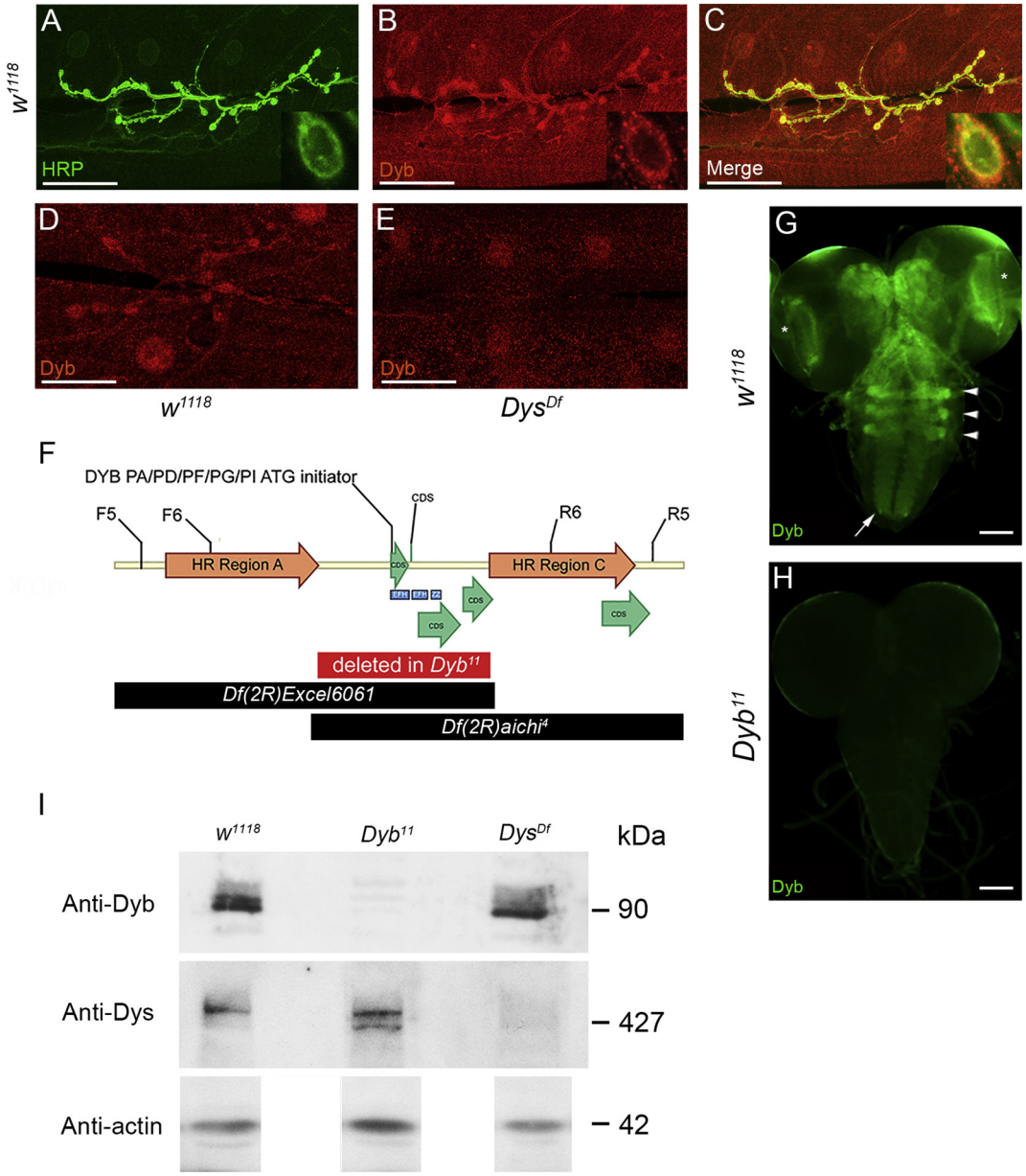

Fig. 1. Dyb is delocalized from the NMJ in the absence of Dys.
Wild-type (w^{1118}) third instar larval body walls were stained with anti-HRP (A), recognizing a presynaptic marker and anti-DybCO_2H (B), with the merged images being shown in (C). High magnification images of a single bouton are shown in the insets at the lower right side of each panel. Anti-DybCO_2H-stained w^{1118} (D) and homozygous Dys^{Df} (E) are shown. The regions used for the donor homologous recombination construct (HR Regions A and C), the initial codon employed by five out of the seven Dyb isoforms, CDS-encoding exons, the regions encoding the EF-Hand and ZZ domains common to all Dyb isoforms, and the locations of the primer hybridizing sites used to confirm the targeting event are shown (F). Anti-DybCO_2H staining of w^{1118} (G) and Dyb^{11}(H) of third instar larval brains/neuropiles is shown. The asterisks, arrow heads, and arrow represent Dyb staining at optic lobes, thoracic neuromeres, and abdominal neuromeres, respectively. Western blot analysis showing Dyb and Dys protein expression in body wall lysates derived from w^{1118}, Dyb^{11}, and Dys^{Df} and compared with the abundance of actin (I). Scale bar = 50 μm.

3.2. Dyb mutants disturb the synaptic ultrastructure and increase bouton numbers due to the absence of the postsynaptic Dyb protein

Since Dyb and Dys are both components of the DGC in mammals [34–36], we investigated whether mutant alleles of *Dys* and *Dyb* interact genetically. *Drosophila* wings typically show a stereotypic pattern with five longitudinal and two crossveins that consist of the anterior crossvein (ACV) and posterior crossvein (PCV). The PCV of the homozygous *Dys* mutant is partially missing, whereas the heterozygous *Dys* mutant has a normal PCV [17]. Homozygous and heterozygous Dyb^{11} wings showed normal PCV formation (Fig. S1A, C, G), similar to heterozygous *Dys* mutant ($Dys^{DLP2\ E6}$) wings (Fig. S1D, G). Homozygous $Dys^{DLP\ E62}$ displayed an alteration in the formation of the PCV by either an absent or failed connection between one or both of the adjacent longitudinal veins (Fig. S1B, G). Simultaneous *Dyb* homozygous and *Dys* heterozygous mutants showed the genetic interaction of these two genes during PCV formation (Fig. S1F, G).

Since we previously observed no change in the overall NMJ structure in the *Dys* mutant [16], we investigated whether Dyb^{11} mutants exhibit the same effect. The overall NMJ structure in the Dyb^{11} mutant was similar to that of the wild-type control; however, synapse size increased (Fig. 2A-B, E-F). The quantitation of bouton numbers at the NMJ visualized by anti-HRP staining revealed an approximately 25% increase in the number of boutons per synapse in the Dyb^{11} mutant

(Fig. 2B, E). Staining data with antibodies recognizing several proteins located at the synapse, including the glutamate receptors DGluRIIA [37] and DGluRIIB [8], the Fas2 protein [38], and SSR-associated scaffolding protein Discs-large (DLG; [39]) revealed that the level and localization of these proteins in the *Dyb*^{11} mutant background were similar to those of the wild type (Fig. S3A–L). We performed neuronal- versus muscle-specific Dyb rescue using OK6-GAL4 and 24B-GAL4 respectively, we found that the postsynaptic, but not presynaptic, expression of Dyb in the *Dyb*^{11} mutant background restored bouton numbers to normal levels (Fig. 2C-D, F) whereas either neuronal- versus muscle-specific Dyb expression alone did not change the bouton numbers (Suppl. Table 4).

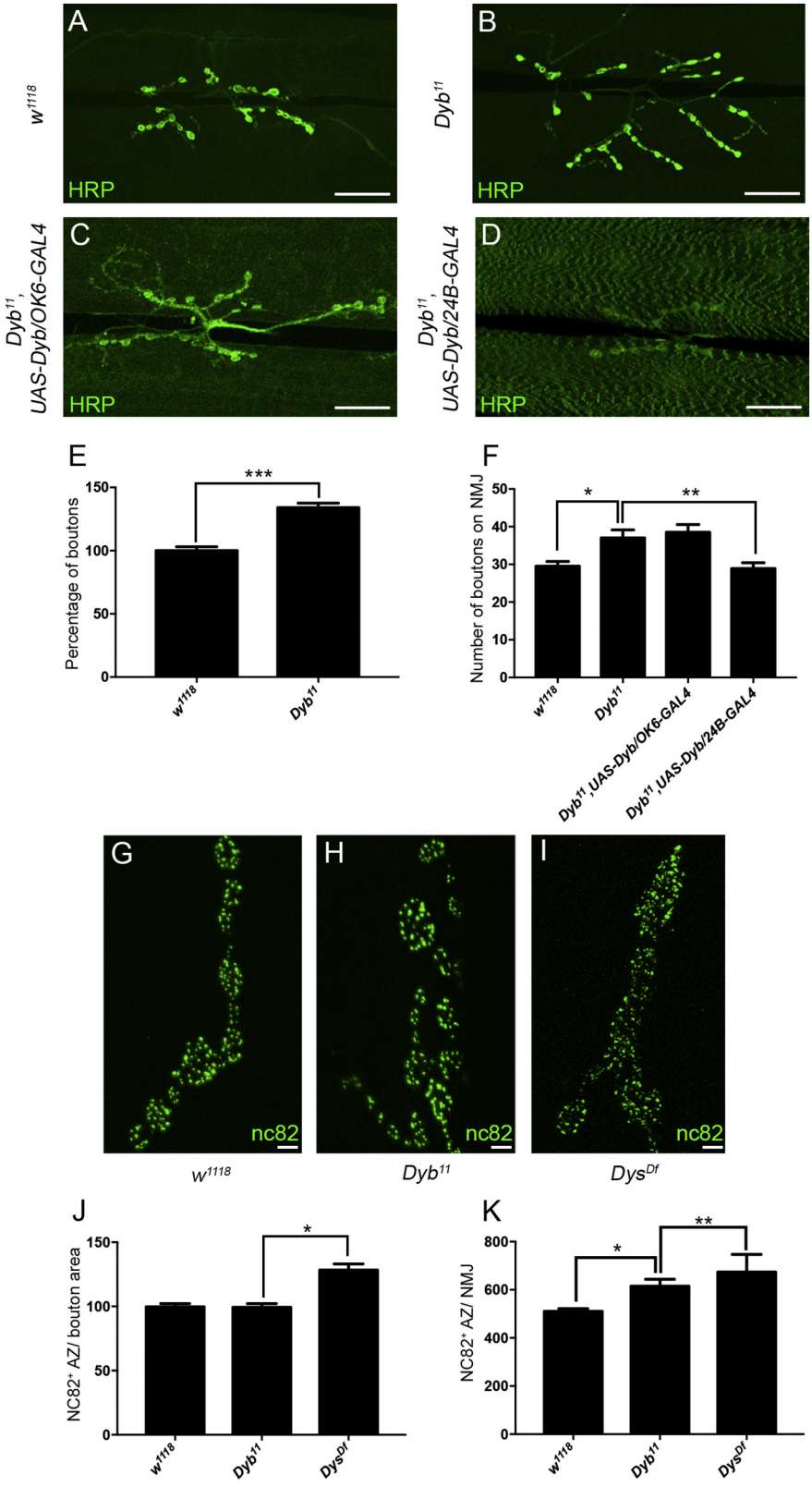

Fig. 2. The *Dyb* mutant displays increased numbers of synaptic boutons, which is rescued by the postsynaptic expression of Dyb and the increased numbers of synaptic nc82^{+} active zones observed in *Dyb* and *Dys* mutants. Wild-type (*w*^{1118}) (A), *Dyb*^{11} mutant (B), *Dyb*^{11}*;UAS-Dyb;OK6-GAL4* (C) and *Dyb*^{11}*;UAS-Dyb;24B-GAL4* (D) synapses at muscle 6/7 visualized with anti-HRP are shown and quantified in (E). The number of boutons at the NMJ was visualized and quantified when Dyb was expressed by using presynaptic (OK6) and postsynaptic (24B)-specific GAL4 drivers, respectively (F). The anti-Bruchpilot (nc82) staining of *w*^{1118} (G), *Dyb*^{11} (H), and *Dys*^{Df} (I) synapses is shown with quantified nc82-positive punctae (nc82^{+} AZ) per bouton area (J) and per total synapses (K). Scale bar of A and B = 25 μm, *E*-F = 5 μm. $n = 15$/each for HRP and NC82 stainings. All data represent mean ± SEM. * $p < 0.05$, ** $p < 0.01$, *** $p < 0.001$.

We examined serial sections of wild-type versus *Dyb*^{11} body walls by TEM to investigate potential changes in the synaptic ultrastructure (Fig. S4A–B). Quantification of the SSR area normalized to the bouton area revealed that the *Dyb*^{11} mutant showed a slight increase in the size of the SSR, an area of a highly folded membrane in the muscle closely associated with the motoneuron terminus (Fig. S4C). Furthermore, we observed a marked increase in apparent patches within the SSR (Fig. S4D) which are worth to further investigation.

The nc82 antibody recognizes Bruchpilot, a component of the presynaptic vesicle-docking T-bar structure [40]. We previously demonstrated that increases in the numbers of nc82^{+} punctae in the *Dys* mutant correlated with the higher number of T-bars visualized by electron microscopy [17]. Anti-Bruchpilot staining was performed on control, *Dyb*^{11} and *Dys*^{Df} mutant larval body walls (Fig. 2G-I). When the total number of nc82^{+} punctae per bouton area was plotted, no significant differences were observed between *Dyb*^{11} and the control; only an increase in nc82^{+} punctae was noted on *Dys*^{Df} (Fig. 2J). However, plotting the total number of nc82^{+} punctae per synapse revealed a significant increase in the number of T-bars per NMJ of *Dyb*^{11} (Fig. 2K), which appeared to reflect the increased number of boutons observed (Fig. 2B, E-F). The absence of Dyb from the muscle resulted in increased numbers of boutons and total release sites per synapse, while the density of release sites within individual boutons remained unaffected.

3.3. The Dyb mutant exhibits enhanced neurotransmitter release, which is rescued by postsynaptic Dyb expression

We evaluated the physiology of the *Dyb*^{11} mutant synapse in current clamping using sharp-electrode recording from the larval NMJ. The *Dyb*^{11} mutant showed a significant increase in the amplitude of evoked junctional potential amplitudes (EJPs) with no apparent differences in miniature EJPs (mEJPs) (Fig. 3A, B; the exact values of all recordings are presented in Suppl. Table 1). This increased the mean QC over that of the control (Fig. 3C; EJP amplitudes, mEJP amplitudes, and mEJP frequencies are shown in Fig. 3D-F). Transheterozygotes bearing independently-derived overlapping deficiencies uncovering the *Dyb* locus (Fig. 1F) displayed similarly increased QC (Fig. 3C). The mutant heterozygous for *Dyb*^{11} also displayed increased QC (Fig. 3C), indicating that *Dyb* is haploinsufficient for this phenotype at the NMJ.

We then investigated whether an increase in the probability of vesicle release underlies increased QC at the *Dyb*^{11} mutant NMJ using PPF. PPF is a form of short-term adaptation of synaptic transmission [41,42] and is quantified by calculations of the ratio of the amplitudes of two consecutive EJPs evoked at short inter-stimulus intervals. When the probability of release of EJP1 decreases, as is observed at lower external Ca^{2+}concentrations, PPF increases. The *Dyb*^{11} mutant was found to display a normal PPF at three Ca^{2+} concentrations when recordings were performed under current-clamp conditions (Fig. 3G). Comparisons of *Dyb*^{11} mutant QCs with those of controls at four external Ca^{2+} concentrations ranging between 0.2 and 1.0 mM revealed no change in the Ca^{2+}cooperativity of neurotransmitter release in the mutant (Fig. 3H). Collectively, these results indicated that a change in presynaptic release probability was not the cause of increased presynaptic release in the *Dyb*^{11} mutant.

To evaluate whether Dyb is required either pre- or postsynaptically to maintain normal neurotransmitter release levels, flies expressing Dyb either pre- or postsynaptically were introduced into the *Dyb*^{11} mutant background. Only postsynaptic Dyb expression on the *Dyb*^{11} mutant rescued QC to normal levels (mean QC shown in Fig. 4A; mean EJP amplitudes, mean mEJP amplitudes, and mean mEJP frequencies are presented in Fig. 4B-D, respectively). Our results indicated that the absence of postsynaptic Dyb was responsible for the increase observed in neurotransmitter release.

3.4. Dyb acts through the Rho-GTPase Cdc42 to regulate presynaptic neurotransmitter release

We previously reported that the increase in QC in the *Dys* mutant was prevented by the presence of a heterozygous null allele of *Cdc42* or by the postsynaptic expression of dsRNA targeting the *cdc42* transcript [17]. These findings indicated that Cdc42 activity was increased in the *Dys* mutant background. We found that the expression of *Cdc42*-specific dsRNA or the heterozygosity of a null mutant allele of *Cdc42* also prevented the increase in QC in the *Dyb*^{11} mutant background (Fig. 5A, mean EJP amplitudes, mean mEJP amplitudes, and mEJP frequencies are shown in Fig. 5B-D). The postsynaptic expression of a constitutively-active Cdc42-encoding transgene (*UAS-Cdc42*^{V12}) alone resulted in elevated QC levels, similar to those observed in *Dys* and *Dyb* mutants (Fig. 5A). Thus, Cdc42 appears to be a primary effector of the postsynaptic Dys/Dyb/Cv-c pathway. We previously employed the heterozygous *Dys* mutant as a sensitized background to uncover a trans-heterozygous *Dys/Cv-c* genetic interaction during PCV formation. The present results also confirmed the genetic interaction between *Dyb* and *Cv-c* (Fig. S5). These genetic interactions during wing vein formation support the possibility that these genes also interact at the NMJ. Moreover, our results showing that Dyb and Cdc42 co-localize in the SSR (Fig. 5E-G) and that Cdc42 appears to be actively concentrated in the SSR, as evidenced by the high level of accumulation of GFP-Cdc42 there when it was expressed in the muscle (Fig. 5H), support the likelihood of interactions between these proteins.

3.5. Rapid synaptic homeostasis is not initiated appropriately in the absence of Dyb

Since Cdc42 was previously shown to be involved in the regulation of synaptic homeostasis at the *Drosophila* neuromuscular synapse [43], we tested whether *Dyb*^{11} mutants exhibit reduced homeostatic responses when challenged with a smaller quantal size. PhTx is a dose-dependent glutamate receptor antagonist that induces a robust homeostatic response when applied to the larval NMJ [7]. We measured evoked and spontaneous EJPs in the presence or absence of PhTx in *Dyb*^{11} mutants and controls. mEJP amplitudes were reduced in controls and *Dyb*^{11} mutants (Fig. 6A-B), indicating that PhTx similarly inhibits postsynaptic glutamate receptors in both genotypes. The wild type showed an increase in presynaptic QC that offset the change in mEJP amplitude and restored EJP amplitudes to control values (Fig. 6A–D). In contrast, EJPs in *Dyb*^{11} mutants with PhTx were significantly smaller than in the absence of PhTx and the homeostatic increase in QC was suppressed (Fig. 6C–D). Since baseline QC was greater than in the controls, two interpretations are possible; either Dyb is required for homeostatic plasticity or an enhanced baseline release in *Dyb* mutants occludes homeostatic plasticity.

3.6. The DGC regulates the RRP of synaptic vesicles

PhTx-induced homeostasis depends on an increase in the RRP of synaptic vesicles [10,30]. To investigate whether the RRP is altered in the *Dyb*^{11} mutant, we employed a two-electrode voltage clamp (TEVC) and stimulated the nerves innervating muscles at 60 Hz in the presence of 1.5 mM calcium [44,45]. We measured RRP in the presence and absence of PhTx. The cumulative EJC amplitude in the control was similar in the presence and absence of PhTx (Fig. 7B, D). When we calculated the RRP size from the cumulative EJP [10,30], we confirmed that the PhTx treatment increased the RRP size to 169% of the baseline in the controls (Fig. 7C). Although the cumulative EJC amplitude in *Dyb*^{11} mutants was significantly larger, the cumulative EJC amplitude decreased when PhTx was applied (Fig. 7B, E), indicating that there was no homeostatic increase in RRP levels in the *Dyb*^{11} mutant (Fig. 7C). To test whether Dyb is required pre- or postsynaptically for homeostatic compensation of the RRP, we performed TEVC with a high frequency

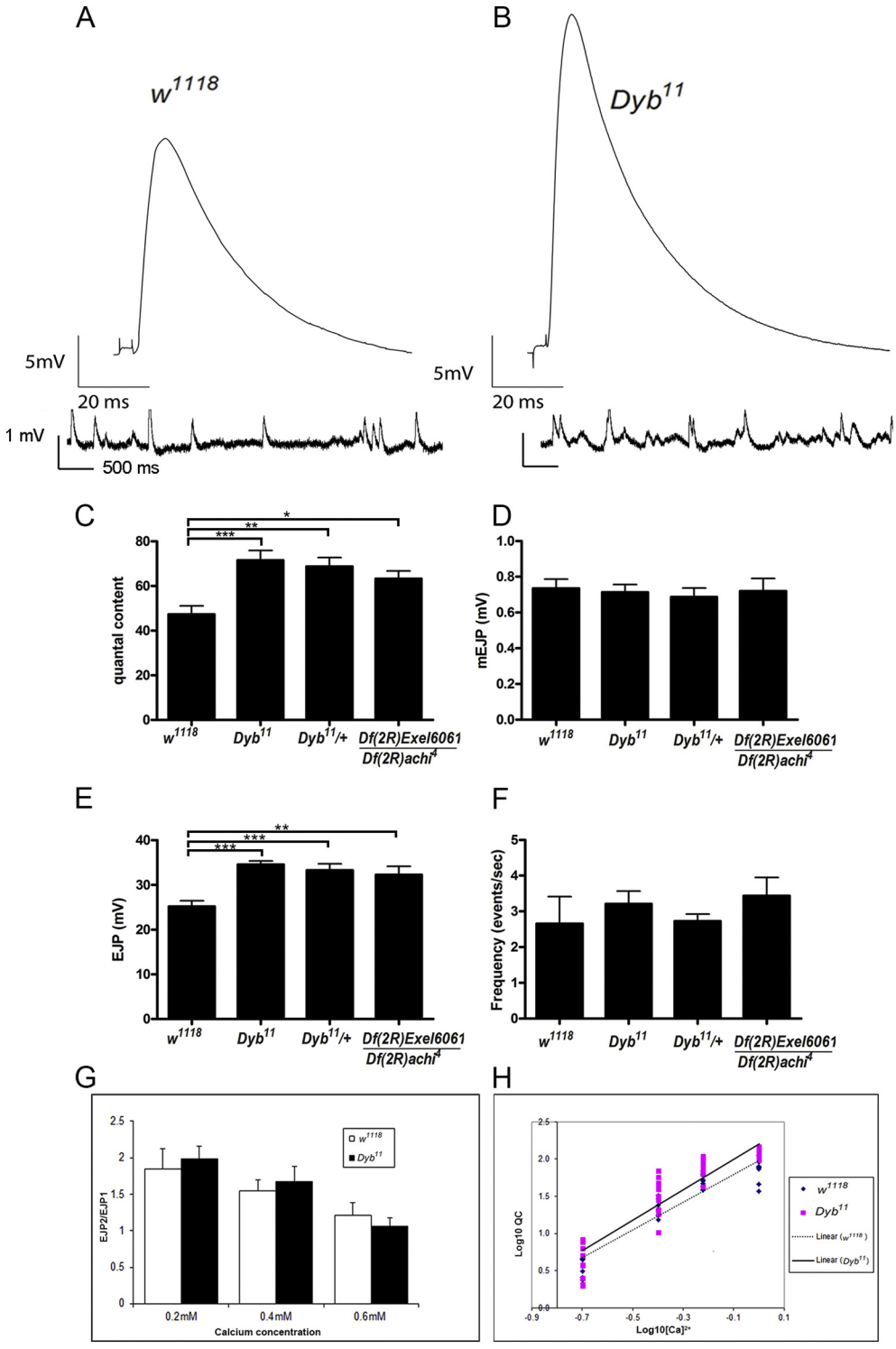

Fig. 3. *Dyb* mutant exhibits increased neurotransmitter release.
Traces of EJP (upper) and mEJP (lower) recordings at wild-type (w^{1118}) (A) and Dyb^{11} mutant (B) synapses are shown. The quantification of QC (C), mEJP amplitudes (D), EJP amplitudes (E), and frequencies (F) are shown for (w^{1118}, $n = 14$), homozygous (Dyb^{11}, $n = 17$), heterozygous ($Dyb^{11}/+$, $n = 10$), and a transheterozygous combination of *Dyb* deficiencies (Df(2R) Exel6061/Dr.(2R)achi^4, $n = 5$), which uncover the *Dyb* genomic locus. The 0.6 mM calcium concentration was used in electrophysiological experiments (A-F). Paired-pulse facilitation analyses were performed at 0.2 mM, 0.4 mM and 0.6 mM of Ca^{2+} concentrations in w^{1118} ($n = 4$, n = 5 and $n = 8$, respectively), Dyb^{11} ($n = 3$, $n = 6$, $n = 7$, respectively) (G) and the response to changes in external Ca^{2+} concentrations (H). All data represent mean ± SEM. * $p < 0.05$, ** $p < 0.01$, *** $p < 0.001$.

stimulation in Dyb^{11} mutants expressing Dyb pre- versus postsynaptically. Only the postsynaptic expression of Dyb was able to rescue the size of the cumulative EJC amplitude as well as the PhTx-induced homeostatic response (Fig. 7B-D, F), indicating that Dyb acts postsynaptically to control homeostasis.

3.7. Relocalization of Dyb to the SSR rescues the Dys mutant physiological phenotype

Since we observed increased neurotransmitter release at the Dyb^{11} mutant NMJ, we hypothesized that the increase in QC in the Dys^{Df} background may be due to the delocalization of Dyb in the absence of Dys. In the Dys^{Df} mutant background, Dyb is delocalized from the sarcomere, indicating that Dyb is anchored by Dys (Fig. 8A–B). We generated fly lines expressing Dyb tagged with an eleven-amino acid sequence derived from the Shaker protein that was previously shown to target heterologous proteins to the SSR [22]. Targeting by this sequence is due to its interaction with DLG, which is localized both pre- and postsynaptically at the NMJ [39]. The tagged protein localizes to boutons in the absence of Dys, and we performed pre- versus

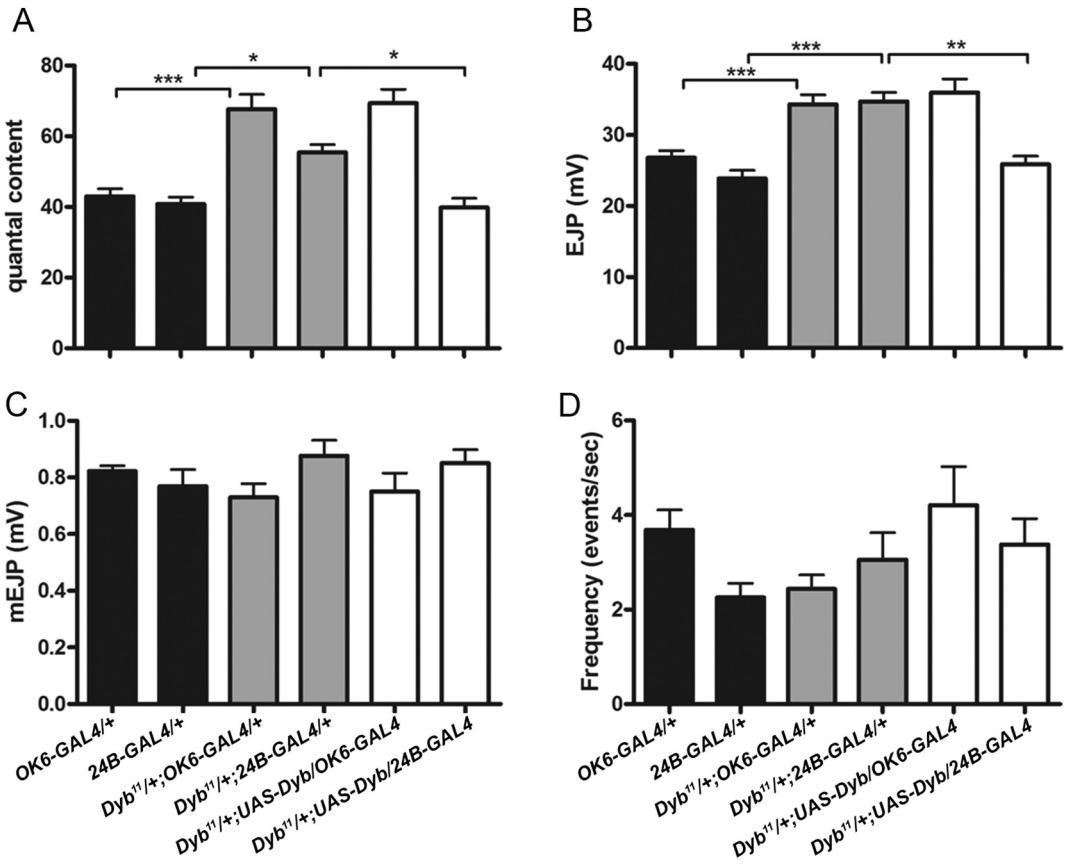

Fig. 4. *Dyb*^{11} mutants increased QC phenotype is rescued by postsynaptic Dyb expression.
Evaluations of the synaptic physiology of synapses at which Dyb is expressed either pre- or postsynaptically in the *Dyb*^{11} mutant background. The QC (A), EJP amplitudes (B), mEJP amplitudes (C), and frequencies (D) for controls *OK6-GAL4/+* ($n = 20$), *24B-GAL4/+* ($n = 11$), heterozygous *Dyb*^{11} mutants *Dyb*^{11}*/+;OK-6-GAL4/+* (n = 10) and *Dyb*^{11}*/+;24B-GAL4/+*(n = 5), presynaptic Dyb expression (*Dyb*^{11}*/+;UAS-Dyb;OK6-GAL4,* n = 10), and postsynaptic Dyb expression (*Dyb*^{11}*/+;UAS-Dyb;24B-GAL4*, n = 8) in the heterozygous mutant background are shown. The 0.6 mM calcium concentration was used in electrophysiological experiments (A–D). All data represent mean ± SEM. * $p < 0.05$, ** $p < 0.01$, *** $p < 0.001$.

postsynaptic rescue experiments in the *Dys*^{Df} mutant background. As expected, when Dyb was expressed under the control of a motoneuron-specific (OK6-GAL4) or muscle-specific GAL4 (24B-GAL4) driver (Fig. 8C–D), the tagged Dyb protein post-, but not pre-synaptically, restored QC to normal levels in the *Dys*^{Df} mutant background (Fig. 8E; EJP amplitudes, mEJP amplitudes, and mEJP frequencies are shown in Fig. 8F–H), demonstrating that the postsynaptic delocalization of Dyb underlies the *Dys*^{Df} mutant QC phenotype. Furthermore, the rescue phenotype of tagged Dyb in the *Dys*^{Df} mutant revealed a role for Dyb in the SSR to rescue the defect in presynaptic neurotransmitter release.

4. Discussion

In the present study, we described a postsynaptic function for DGC within the SSR that influences synaptic strength and homeostatic plasticity at the *Drosophila* NMJ. We found that Dyb was present in pre- and postsynaptic compartments at the NMJ and its localization required Dys. Dyb is localized in the larval neuropile in a pattern that is very similar to that of the CNS-specific Dys Dp186 isoform, which is required in an identified motoneuron to regulate neurotransmitter release by upstream cholinergic interneurons [46]. Thus, Dyb may also be proved to be part of a DGC-like complex in postsynaptic motoneuron dendrites.

It currently remains unclear whether Dp186 is involved in homeostatic mechanisms at this inter-neuronal synapse. Collectively, the findings of fly and mammalian studies support the possibility that the DGC is engaged in homeostatic plasticity at various types of synapses and, if so, may reasonably be involved in the common mechanisms of detecting perturbations within postsynaptic neurons.

Studies on Dys-deficient rodent hippocampal neurons revealed the up-regulation of presynaptic neurotransmitter release [47,48] with accompanying morphological alterations in the presynaptic compartment [49,50], which is consistent with the present results obtained at the *Drosophila* NMJ. However, a recent study implicated the DGC in a different form of homeostatic plasticity in the mammalian CNS [51].

Since the transmembrane DG protein provides the DGC's anchor in the membrane and its absence results in the delocalization of DGC components, the absence of Dyb may also, at least partially, contribute to this form of homeostatic plasticity. A previous study consistently showed that mice lacking both Dyb isoforms (DTNA and DTNB), but not either alone, displayed a significant reduction in $GABA_A\alpha1$ foci at cerebellar inhibitory synapses [52. However, this homeostatic plasticity differs from our *Drosophila* NMJ homeostatic studies because we did not observe any morphological or functional changes in the postsynaptic receptor field in DGC mutants (this work and [16,17]).

Dyb mutants do not display increased QC when challenged with PhTx. This disruption of presynaptic homeostasis is associated with the failure to modulate the RRP. The failure to modulate the RRP in a *RIM* mutant background was previously shown to correlate with impaired presynaptic homeostasis [10]. The difference between *Dyb*^{11} and *RIM* mutations is that the *Dyb*, but not *RIM*, mutant displays an increase in presynaptic release at baseline; this effect correlates with an increase in the number of presynaptic active zones. Since the *Dyb* mutant does not display impaired PPF, we attributed enhanced basal neurotransmitter release to an increase in the active zone number, not a change in release probability. Similarly, we previously demonstrated that *Cv-c* mutants did not exhibit increased PPF [17] supporting the idea that the DGC-

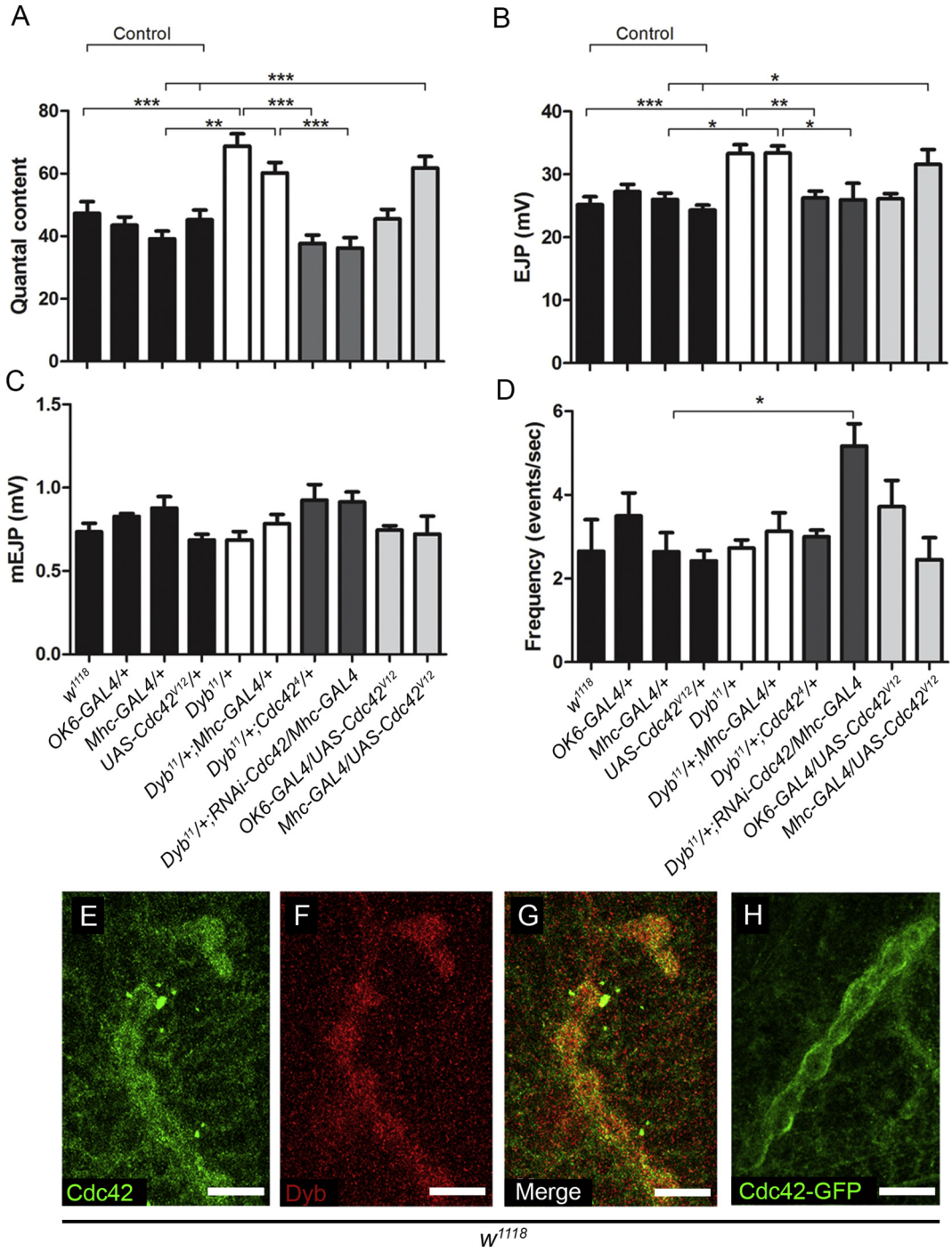

Fig. 5. Reduction in Cdc42 expression levels rescues the *Dyb* mutant increased QC phenotype and the postsynaptic expression of constitutively-active Cdc42 phenocopies of the *Dyb* mutant phenotype.

Electrophysiological recordings of controls w^{1118} (n = 5), *OK6-GAL4/+* (*n* = 15), *Mhc-GAL4/+* (n = 8), *UAS-Cdc42*^{V12}*/+* (n = 6), heterozygous Dyb^{11} mutants $Dyb^{11}/+$ (*n* = 10) and $Dyb^{11}/+$*;Mhc-GAL4/+* (n = 7), heterozygous Dyb^{11} *and* $Cdc42^{4}$ mutants ($Dyb^{11}/+;Cdc42^{4}/+$, n = 6), postsynaptic *Cdc42* knockdown on the Dyb^{11} mutant background ($Dyb^{11}/+$*;RNAi-Cdc42/Mhc-GAL4* n = 5), the presynaptic expression of Cdc42 (*OK6-GAL4/UAS-Cdc42*^{V12}, n = 6), and the postsynaptic expression of Cdc42 (*Mhc-GAL4/UAS-Cdc42*^{V12}, n = 6) were quantified. QC (A), EJP amplitudes (B), mEJP amplitudes (C), and frequencies (D) of the indicated genotypes are shown. Wild-type (w^{1118}) third instar larval body walls were stained with anti-Cdc42 (E) and anti-DybCO_2H (F), with the merged image shown in (G). The accumulation of overexpressed GFP-Cdc42 in the SSR is shown in (H). The 0.6 mM calcium concentration was used in electrophysiological experiments. Scale bar = 10 μm. All data represent mean ± SEM. * $p < 0.05$, ** $p < 0.01$, *** $p < 0.001$.

mediated pathway does not regulate the probability of release.

The QC elevation can be caused by either increased probability of release or increased RRP size. Our group previously reported that an elevation in evoked neurotransmitter release in *Dys* mutant was because of an increased probability of release rather than an increased size of RRP [16]. Although Dys and Dyb have been found to interact, the causative of an elevation on evoked neurotransmitter release was likely different. In the present study, *Dyb* mutant did not increase in probability of release but it showed the defect in the RRP modulation after PhTx administration. However, the methods of RRP determination

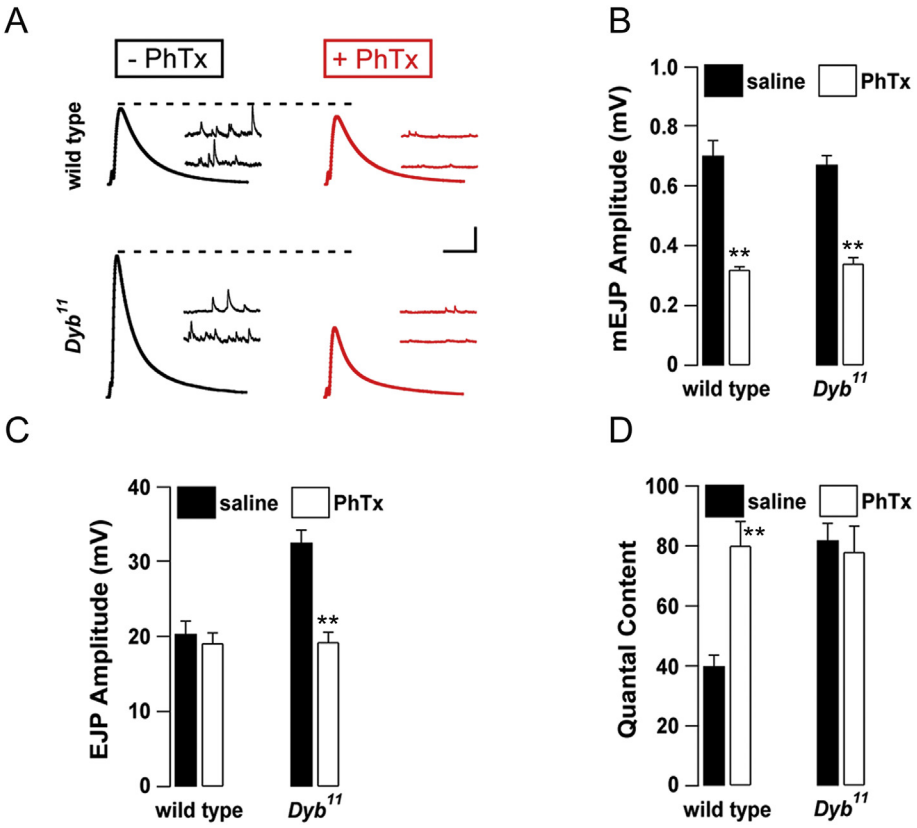

Fig. 6. Dyb is essential for rapid homeostatic potentiation.
(A) Sample traces showing EJP and mEJP amplitudes for w^{1118} (upper) and Dyb^{11} (lower) in the presence or absence of PhTx (red and black, respectively). (B) Average mEJP amplitudes for the indicated genotypes in saline (black bars) or saline with PhTx (white bars). Average EJP amplitude (C) and QC (D). EJP amplitudes were quantified by comparisons to the baseline in both genotypes. The 0.5 mM calcium concentration was used in electrophysiological experiments. Scale bars for EJPs = 5 mV, vertical, and 100 ms, horizontal. Scale bars for mEJPs = 2 mV, vertical, and 1 s, horizontal. All data represent mean ± SEM. ** $p < 0.01$. $n = 10$/each group.

between these two studies were likely different (this work and [16]), these might affect an interpretation of the results.

The restoration of Dyb into a postsynaptic, but not a presynaptic, compartment in the *Dys* mutant background suppressed the high QC phenotype of the *Dys* mutant. These results confirmed that the loss of Dyb from the SSR, which is regarded as a postsynaptic compartment, in the *Dys* mutant background enhanced presynaptic release. Further studies are warranted to more clearly understand how DGC members

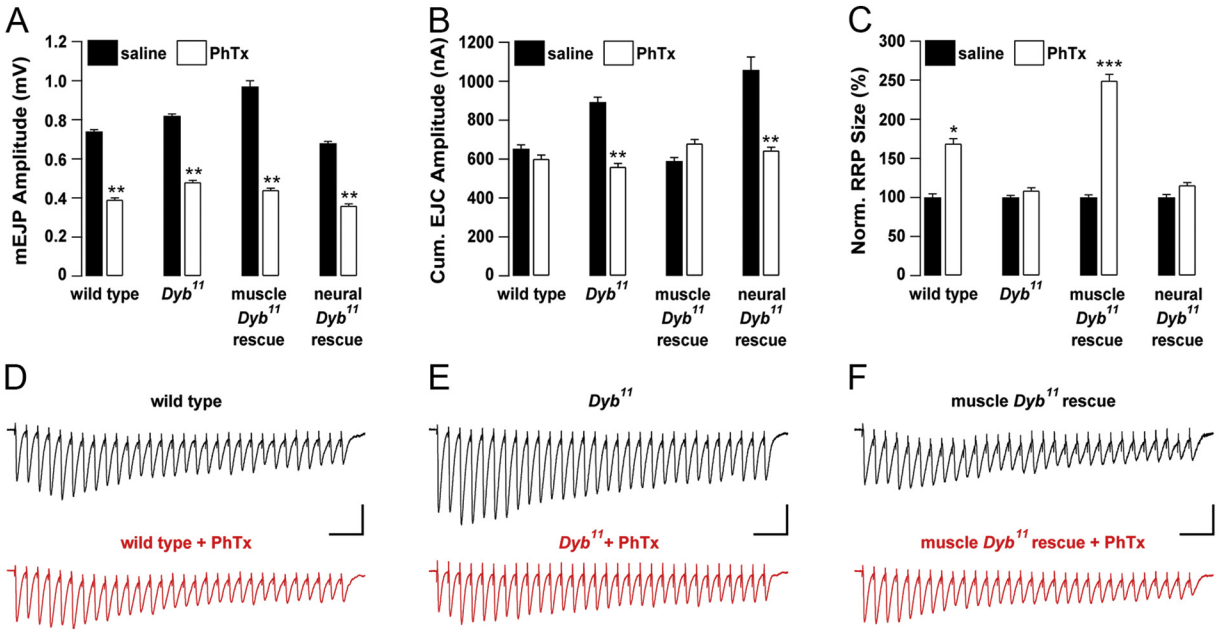

Fig. 7. Dyb is required postsynaptically for the modulation of RRP sizes during rapid homeostatic potentiation.
(A) Average mEJP amplitudes for w^{1118}, Dyb^{11}, presynaptic Dyb rescue ($Dyb^{11}/+$;*UAS-Dyb;OK6-GAL4*), and postsynaptic Dyb rescue ($Dyb^{11}/+$;*UAS-Dyb;24B-GAL4*) in saline (black) or saline with PhTx (white) are shown. (B) Average cumulative (Cum.) EJC amplitudes. (C) Average normalized (Norm.) RRP sizes were shown as percentages. All data represent mean ± SEM. (D-F) Sample traces showing EJC amplitudes, evoked by a 60-Hz stimulation in 1.5 mM Ca^{2+}, for w^{1118}, Dyb^{11}, and muscle Dyb^{11} rescue in the presence (bottom, red) and absence (top, black) of PhTx. Scale bars = 50 nA, vertical, and 50 ms, horizontal. All data represent mean ± SEM. * $p < 0.05$, ** $p < 0.01$. n = 10/each group.

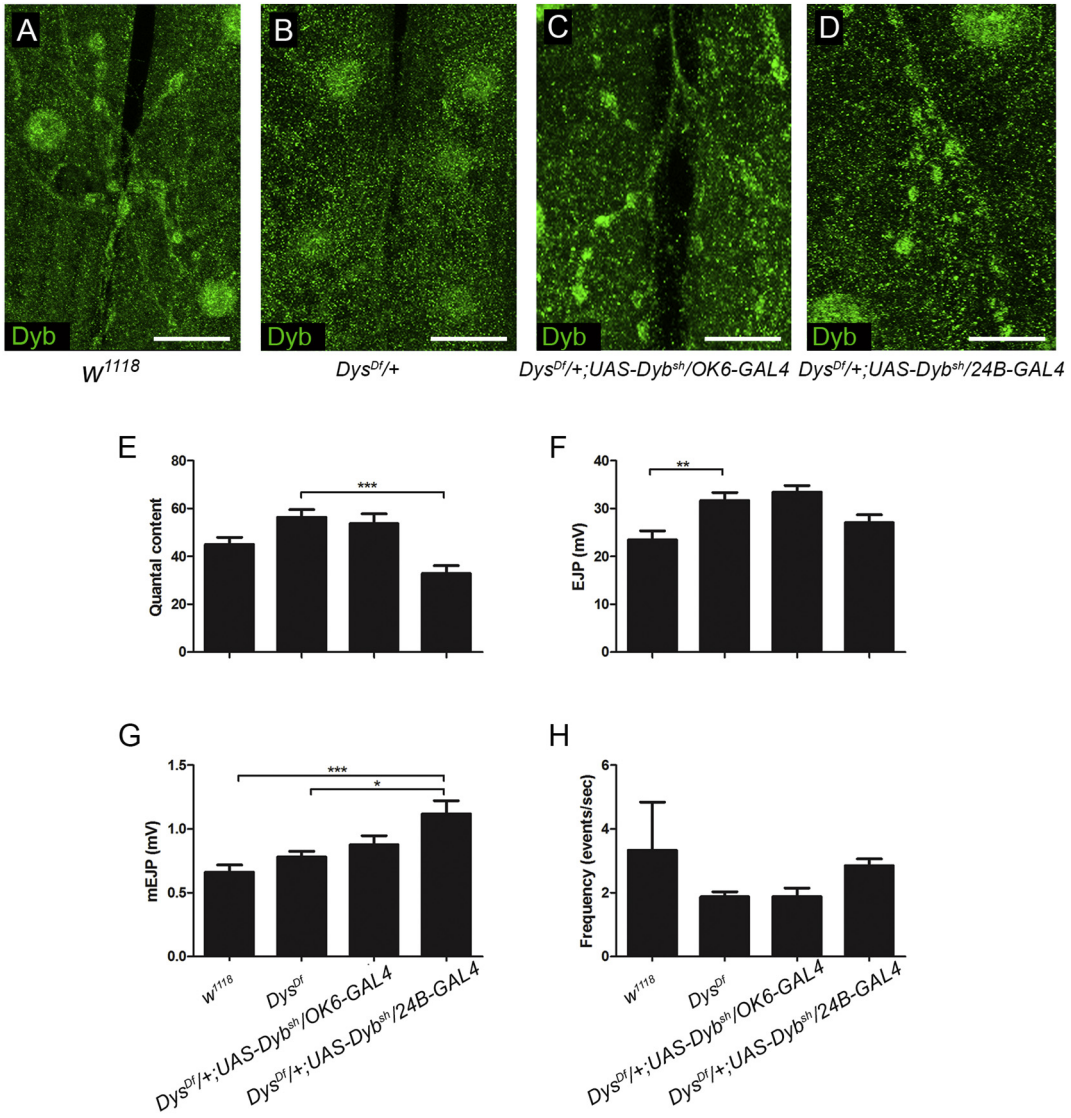

Fig. 8. Dyb is delocalized from Dys^{Df} synapses and the relocalization of Dyb to postsynaptic regions of Dys^{Df} boutons rescues the high QC phenotype of Dys^{Df}. The Dyb expression of w^{1118} (A), $Dys^{Df}/+$ (B), $Dys^{Df}/+$;*UAS-Dyb^{sh}/OK6-GAL4* (C), and $Dys^{Df}/+$;*UAS-Dyb^{sh}/OK6-GAL4* (D) was observed on muscle 6/7 synapses. The electrophysiological recordings of QC (E), EJP amplitudes (F), mEJP amplitudes (G), and frequencies (H) representing each group are shown. w^{1118} and $Dys^{Df}/+$ (n = 7/each), $Dys^{Df}/+$;*UAS-Dyb^{sh}/OK6-GAL4* (n = 5) and $Dys^{Df}/+$;*UAS-Dyb^{sh}/OK6-GAL4* (n = 6) for electrophysiological experiments. Scale bar = 25 μm. All data represent mean ± SEM. * $p < 0.05$, *** $p < 0.001$.

collaboratively function and, in the case of their dysfunction, affect neurons, muscles, and other tissues. The roles of Dyb in the presynaptic compartment currently remain unclear. However, postsynaptic Dyb appears to be mainly involved in the regulation of bouton numbers, QC, and homeostatic plasticity. We were able to rescue these *Dyb* mutant phenotypes solely by the postsynaptic expression of Dyb.

The significance of Rho signaling in maintaining synaptic function is underscored by the identification of a number of human Rho gene-associated mutations underlying cognitive deficit syndromes [53]. Interestingly, the Rho GTPase Cdc42 has also been shown to play a presynaptic role in homeostasis at the NMJ. It acts downstream of the Eph receptor-binding Ephexin protein as a member of a pathway that modulates presynaptic CaV2.1 channels during the homeostatic enhancement of presynaptic release [43]. Collectively, the present results contribute to elucidating the mechanism of action of the DGC complex in the regulation of neurotransmitter release, which is schematically depicted in Fig. S6, in which the postsynaptic DGC complex at the NMJ organizes Rho-GTPase signaling with effects on both presynaptic neurotransmitter release and presynaptic homeostasis. The present results contribute to a better understanding of the likely evolutionarily conserved postsynaptic roles of the DGC in synaptic homeostasis.

Supplementary data to this article can be found online at https://doi.org/10.1016/j.bbadis.2019.03.008.

Transparency document

The Transparency document associated with this article can be found, in online version.

Acknowledgments

We thank Mariska van der Plas and Anneke Kremer for generating the UAS-Dyb constructs and their preliminary characterization of the transformants and anti-DYB antisera, Gonneke Pilgram for her contributions to the early part of this work, James Ashley for suggesting the use of the Shaker SSR-targeting tag, Bert van Veen and Ben de Koster for assistance with the fly work, Monique Bansraj and Niels de Water for assistance with molecular biology, and Anja de Jong for help with

the fly work and immunostaining. We are grateful to A. Chiba, A. DiAntonio, A. Hofbauer, M. Kelley, U. Tepass, R. White, the Developmental Studies Hybridoma Bank, the Bloomington *Drosophila* Stock Center, and the *Drosophila* Genomics Resource Center for kindly providing fly lines, antibodies and plasmids. We thank Isabel de Ridder, Jaap Plomp, and Patrik Verstreken for their comments on earlier versions of this manuscript. We thank Medical English Service for the English language review and Grant-in-Aid from JSPS Core-to-Core Program, B. Asia-Africa Science Platforms.

Fundings

This work was supported by grants from the "Nederlandse Organisatie voor Wetenschappelijk Onderzoek, N. W.O." (J. N. N. and L. G. F.). We also are thankful for the supports from Research Center of Pharmaceutical Nanotechnology, Chiang Mai University, Thailand (S.P., W.N.), Faculty of Medicine, Chiang Mai University (SP), Thailand Research Fund (MRG6180078:SP) and partially supported by Chiang Mai University.

References

[1] G.W. Davis, Homeostatic control of neural activity: from phenomenology to molecular design, Annu. Rev. Neurosci. 29 (2006) 307–323, https://doi.org/10.1146/annurev.neuro.28.061604.135751.
[2] E. Marder, J.M. Goaillard, Variability, compensation and homeostasis in neuron and network function, Nat. Rev. Neurosci. 7 (2006) 563–574, https://doi.org/10.1038/nrn1949.
[3] K. Pozo, Y. Goda, Unraveling mechanisms of homeostatic synaptic plasticity, Neuron. 66 (2010) 337–351, https://doi.org/10.1016/j.neuron.2010.04.028.
[4] S. Bergquist, D.K. Dickman, G.W. Davis, A hierarchy of cell intrinsic and target-derived homeostatic signaling, Neuron. 66 (2010) 220–234, https://doi.org/10.1016/j.neuron.2010.03.023.
[5] A. Maffei, G.G. Turrigiano, Multiple modes of network homeostasis in visual cortical layer 2/3, J. Neurosci. 28 (2008) 4377–4384, https://doi.org/10.1523/JNEUROSCI.5298-07.2008.
[6] G.G. Turrigiano, S.B. Nelson, Hebb and homeostasis in neuronal plasticity, Curr. Opin. Neurobiol. 10 (2000) 358–364, https://doi.org/10.1016/S0959-4388(00)00091-X.
[7] C.A. Frank, M.J. Kennedy, C.P.P. Goold, K.W. Marek, G.W.W. Davis, Mechanisms underlying the rapid induction and sustained expression of synaptic homeostasis, Neuron. 52 (2006) 663–677, https://doi.org/10.1016/j.neuron.2006.09.029.
[8] S.A. Petersen, R.D. Fetter, J.N. Noordermeer, C.S. Goodman, A. DiAntonio, Genetic analysis of glutamate receptors in *Drosophila* reveals a retrograde signal regulating presynaptic transmitter release, Neuron. 19 (1997) 1237–1248, https://doi.org/10.1016/S0896-6273(00)80415-8.
[9] M. Müller, E.C.G. Pym, A. Tong, G.W. Davis, Rab3-GAP controls the progression of synaptic homeostasis at a late stage of vesicle release, Neuron. 69 (2011) 749–762, https://doi.org/10.1016/j.neuron.2011.01.025.
[10] M. Müller, K.S.Y. Liu, S.J. Sigrist, G.W. Davis, RIM controls homeostatic plasticity through modulation of the readily-releasable vesicle pool, J. Neurosci. 32 (2012) 16574–16585, https://doi.org/10.1523/JNEUROSCI.0981-12.2012.
[11] D.K. Dickman, G.W. Davis, The schizophrenia susceptibility gene dysbindin controls synaptic homeostasis, Science 326 (2009) 1127–1130, https://doi.org/10.1126/science.1179685 80-..
[12] M.A. Younger, M. Müller, A. Tong, E.C. Pym, G.W. Davis, A presynaptic ENaC channel drives homeostatic plasticity, Neuron. 79 (2013) 1183–1196, https://doi.org/10.1016/j.neuron.2013.06.048.
[13] C.A. Frank, Homeostatic plasticity at the *Drosophila* neuromuscular junction, Neuropharmacology. 78 (2014) 63–74, https://doi.org/10.1016/j.neuropharm.2013.06.015.
[14] D.J. Blake, Dystrobrevin dynamics in muscle-cell signalling: a possible target for therapeutic intervention in Duchenne muscular dystrophy? Neuromuscul. Disord. (2002) (doi:10.1016/S0960-8966(02)00091-3).
[15] E.P. Hoffman, R.H. Brown, L.M. Kunkel, Dystrophin: the protein product of the duchenne muscular dystrophy locus, Cell. 51 (1987) 919–928, https://doi.org/10.1016/0092-8674(87)90579-4.
[16] M.C. van der Plas, Dystrophin is required for appropriate retrograde control of neurotransmitter release at the *Drosophila* neuromuscular junction, J. Neurosci. 26 (2006) 333–344, https://doi.org/10.1523/JNEUROSCI.4069-05.2006.
[17] G.S.K. Pilgram, S. Potikanond, M.C. van der Plas, L.G. Fradkin, J.N. Noordermeer, The RhoGAP crossveinless-c interacts with dystrophin and is required for synaptic homeostasis at the *Drosophila* neuromuscular junction, J. Neurosci. 31 (2011) 492–500, https://doi.org/10.1523/JNEUROSCI.4732-10.2011.
[18] A.B. Jaffe, A. Hall, RHO GTPASES: biochemistry and biology, Annu. Rev. Cell Dev. Biol. 21 (2005) 247–269, https://doi.org/10.1146/annurev.cellbio.21.020604.150721.
[19] R.G. Fehon, T. Oren, D.R. LaJeunesse, T.E. Melby, B.M. McCartney, Isolation of mutations in the *Drosophila* homologues of the human Neurofibromatosis 2 and yeast CDC42 genes using a simple and efficient reverse-genetic method, Genetics. 146 (1997) 245–252 http://www.ncbi.nlm.nih.gov/pubmed/9136014 , Accessed date: 14 November 2018.
[20] L. Luo, Y.J. Liao, L.Y. Jan, Y.N. Jan, Distinct morphogenetic functions of similar small GTPases: *Drosophila* Drac1 is involved in axonal outgrowth and myoblast fusion, Genes Dev. 8 (1994) 1787–1802 http://www.ncbi.nlm.nih.gov/pubmed/7958857 (accessed November 14, 2018).
[21] D. Kamiyama, A. Chiba, Endogenous activation patterns of Cdc42 GTPase within *Drosophila* embryos, Science (80-.). 324 (2009) 1338–1340. doi:https://doi.org/10.1126/science.1170615.
[22] K. Zito, R.D. Fetter, C.S. Goodman, E.Y. Isacoff, Synaptic clustering of Fasciclin II and shaker: essential targeting sequences and role of Dlg, Neuron. 19 (1997) 1007–1016, https://doi.org/10.1016/S0896-6273(00)80393-1.
[23] W.J. Gong, K.G. Golic, Ends-out, or replacement, gene targeting in *Drosophila*, Proc. Natl. Acad. Sci. 100 (2003) 2556–2561, https://doi.org/10.1073/pnas.0535280100.
[24] S.B. Marrus, S.L. Portman, M.J. Allen, K.G. Moffat, A. DiAntonio, Differential localization of glutamate receptor subunits at the *Drosophila* neuromuscular junction, J. Neurosci. 24 (2004) 1406–1415 (doi:10.1523/JNEUROSCI.1575-03.2004).
[25] K.P. Harris, U. Tepass, Cdc42 and Par proteins stabilize dynamic adherens junctions in the *Drosophila* neuroectoderm through regulation of apical endocytosis, J. Cell Biol. 183 (2008) 1129–1143, https://doi.org/10.1083/jcb.200807020.
[26] C.M. Schuster, G.W. Davis, R.D. Fetter, C.S. Goodman, Genetic dissection of structural and functional components of synaptic plasticity. II. Fasciclin II controls presynaptic structural plasticity, Neuron. 17 (1996) 655–667, https://doi.org/10.1016/S0896-6273(00)80198-1.
[27] A. Hofbauer, T. Ebel, B. Waltenspiel, P. Oswald, Y.C. Chen, P. Halder, S. Biskup, U. Lewandrowski, C. Winkler, A. Sickmann, S. Buchner, E. Buchner, The Wuerzburg hybridoma library against *Drosophila* brain, J. Neurogenet. 23 (2009) 78–91, https://doi.org/10.1080/01677060802471627.
[28] A.R. Martin, A further study of the statistical composition of the end-plate potential, J. Physiol. 130 (1955) 114–122, https://doi.org/10.1113/jphysiol.1955.sp005397.
[29] R. Schneggenburger, A.C. Meyer, E. Neher, Released fraction and total size of a pool of immediately available transmitter quanta at a calyx synapse, Neuron. 23 (1999) 399–409, https://doi.org/10.1016/S0896-6273(00)80789-8.
[30] A. Weyhersmuller, S. Hallermann, N. Wagner, J. Eilers, Rapid active zone remodeling during synaptic plasticity, J. Neurosci. 31 (2011) 6041–6052, https://doi.org/10.1523/JNEUROSCI.6698-10.2011.
[31] L.C. Dekkers, M.C. van der Plas, P.B. van Loenen, J.T. den Dunnen, G.J.B. van Ommen, L.G. Fradkin, J.N. Noordermeer, Embryonic expression patterns of the *Drosophila* dystrophin-associated glycoprotein complex orthologs, Gene Expr. Patterns 4 (2004) 153–159, https://doi.org/10.1016/j.modgep.2003.09.004.
[32] L.Y. Jan, Y.N. Jan, Antibodies to horseradish peroxidase as specific neuronal markers in *Drosophila* and in grasshopper embryos, Proc. Natl. Acad. Sci. 79 (1982) 2700–2704, https://doi.org/10.1073/pnas.79.8.2700.
[33] W. Chung, J.T. Campanelli, WW and EF hand domains of dystrophin-family proteins mediate dystroglycan binding, Mol. Cell Biol. Res. Commun. 2 (1999) 162–171, https://doi.org/10.1006/mcbr.1999.0168.
[34] C. Perronnet, C. Vaillend, Dystrophins, utrophins, and associated scaffolding complexes: role in mammalian brain and implications for therapeutic strategies, J Biomed Biotechnol 2010 (2010) 849426, , https://doi.org/10.1155/2010/849426.
[35] J. Strakova, J.D. Dean, K.M. Sharpe, T.A. Meyers, G.L. Odom, D. Townsend, Dystrobrevin increases dystrophin's binding to the dystrophin–glycoprotein complex and provides protection during cardiac stress, J. Mol. Cell. Cardiol. 76 (2014) 106–115, https://doi.org/10.1016/j.yjmcc.2014.08.013.
[36] B. Constantin, Dystrophin complex functions as a scaffold for signalling proteins, Biochim. Biophys. Acta Biomembr. 1838 (2014) 635–642, https://doi.org/10.1016/j.bbamem.2013.08.023.
[37] C.M. Schuster, A. Ultsch, P. Schloss, J.A. Cox, B. Schmitt, H. Betz, Molecular cloning of an invertebrate glutamate receptor subunit expressed in *Drosophila* muscle., Science (80-.). 254 (1991) 112–114. doi:https://doi.org/10.1126/science.1681587.
[38] G. Grenningloh, E. Jay Rehm, C.S. Goodman, Genetic analysis of growth cone guidance in *Drosophila*: Fasciclin II functions as a neuronal recognition molecule, Cell. 67 (1991) 45–57, https://doi.org/10.1016/0092-8674(91)90571-F.
[39] T. Lahey, M. Gorczyca, X.X. Jia, V. Budnik, The *Drosophila* tumor suppressor gene dlg is required for normal synaptic bouton structure, Neuron. 13 (1994) 823–835, https://doi.org/10.1016/0896-6273(94)90249-6.
[40] D.A. Wagh, T.M. Rasse, E. Asan, A. Hofbauer, I. Schwenkert, H. Dürrbeck, S. Buchner, M.C. Dabauvalle, M. Schmidt, G. Qin, C. Wichmann, R. Kittel, S.J. Sigrist, E. Buchner, Bruchpilot, a protein with homology to ELKS/CAST, is required for structural integrity and function of synaptic active zones in *Drosophila*, Neuron. 49 (2006) 833–844, https://doi.org/10.1016/j.neuron.2006.02.008.
[41] J. Rohrbough, S. Pinto, R.M. Mihalek, T. Tully, K. Broadie, latheo, a *Drosophila* gene involved in learning, regulates functional synaptic plasticity, Neuron. 23 (1999) 55–70, https://doi.org/10.1016/S0896-6273(00)80753-9.
[42] D.J. Sandstrom, Isoflurane depresses glutamate release by reducing neuronal excitability at the *Drosophila* neuromuscular junction, J. Physiol. 558 (2004) 489–502, https://doi.org/10.1113/jphysiol.2004.065748.
[43] C.A. Frank, J. Pielage, G.W. Davis, A presynaptic homeostatic signaling system composed of the Eph receptor, Ephexin, Cdc42, and CaV2.1 calcium channels, Neuron. 61 (2009) 556–569, https://doi.org/10.1016/j.neuron.2008.12.028.
[44] S. Hallermann, M. Heckmann, R.J. Kittel, Mechanisms of short-term plasticity at neuromuscular active zones of *Drosophila*, HFSP J. 4 (2010) 72–84, https://doi.org/10.2976/1.3338710.
[45] K. Miśkiewicz, L.E. Jose, A. Bento-Abreu, M. Fislage, I. Taes, J. Kasprowicz, J. Swerts, S. Sigrist, W. Versées, W. Robberecht, P. Verstreken, ELP3 controls active

zone morphology by acetylating the ELKS family member bruchpilot, Neuron. 72 (2011) 776–788, https://doi.org/10.1016/j.neuron.2011.10.010.

[46] L.G. Fradkin, R.A. Baines, M.C. van der Plas, J.N. Noordermeer, The dystrophin Dp186 isoform regulates neurotransmitter release at a central synapse in *Drosophila*, J. Neurosci. 28 (2008) 5105–5114, https://doi.org/10.1523/JNEUROSCI.4950-07.2008.

[47] F. Daoud, A. Candelario-Martínez, J.M. Billard, A. Avital, M. Khelfaoui, Y. Rozenvald, M. Guegan, D. Mornet, D. Jaillard, U. Nudel, J. Chelly, D. Martínez-Rojas, S. Laroche, D. Yaffe, C. Vaillend, Role of mental retardation-associated dystrophin-gene product Dp71 in excitatory synapse organization, synaptic plasticity and behavioral functions, PLoS One 4 (2009), https://doi.org/10.1371/journal.pone.0006574.

[48] S.F. Parames, E.D. Coletta-Yudice, F.M. Nogueira, M.B. Nering de Sousa, M.A. Hayashi, M.T.R. Lima-Landman, A.J. Lapa, C. Souccar, Altered acetylcholine release in the hippocampus of dystrophin-deficient mice, Neuroscience. 269 (2014) 173–183, https://doi.org/10.1016/j.neuroscience.2014.03.050.

[49] R. Miranda, C. Sébrié, J. Degrouard, B. Gillet, D. Jaillard, S. Laroche, C. Vaillend, Reorganization of inhibitory synapses and increased PSD length of perforated excitatory synapses in hippocampal area CA1 of dystrophin-deficient mdx mice, Cereb. Cortex 19 (2009) 876–888, https://doi.org/10.1093/cercor/bhn135.

[50] R. Miranda, U. Nudel, S. Laroche, C. Vaillend, Altered presynaptic ultrastructure in excitatory hippocampal synapses of mice lacking dystrophins Dp427 or Dp71, Neurobiol. Dis. 43 (2011) 134–141, https://doi.org/10.1016/j.nbd.2011.02.017.

[51] H. Pribiag, H. Peng, W.A. Shah, D. Stellwagen, S. Carbonetto, Dystroglycan mediates homeostatic synaptic plasticity at GABAergic synapses, Proc. Natl. Acad. Sci. 111 (2014) 6810–6815, https://doi.org/10.1073/pnas.1321774111.

[52] R.M. Grady, Cerebellar synaptic defects and abnormal motor behavior in mice lacking- and beta-Dystrobrevin, J. Neurosci. 26 (2006) 2841–2851, https://doi.org/10.1523/JNEUROSCI.4823-05.2006.

[53] S.E. Newey, V. Velamoor, E.E. Govek, L. Van Aelst, Rho GTPases, dendritic structure, and mental retardation, J. Neurobiol. 64 (2005) 58–74, https://doi.org/10.1002/neu.20153.